








## Research Article

# Metal-Organic Framework-Derived Solid Catalyst for Biodiesel Production from *Jatropha curcas* Oil: Kinetic Study and Process Optimization Using Response Surface Methodology

Hlawancheu Zohmingliana <sup>1</sup>, Joseph V. L. Ruatpuia <sup>1</sup>, Jasha Momo H. Anal <sup>2</sup>,  
Feng Chai <sup>3</sup>, Gopinath Halder <sup>4</sup>, Amarajothi Dhakshinamoorthy <sup>5</sup>,  
and Samuel Lalthazuala Rokhum <sup>1</sup>

<sup>1</sup>Department of Chemistry, National Institute of Technology Silchar, Silchar, Assam 788010, India

<sup>2</sup>Natural Products and Medicinal Chemistry Division, CSIR-Indian Institute of Integrative Medicine, Jammu 180001, India

<sup>3</sup>Department of Chemistry, Harbin Normal University, Harbin 150025, China

<sup>4</sup>Department of Chemical Engineering, National Institute of Technology Durgapur, Durgapur 713209, West Bengal, India

<sup>5</sup>School of Chemistry, Madurai Kamaraj University, Madurai 625021, India

Correspondence should be addressed to Samuel Lalthazuala Rokhum; [rokhum@che.nits.ac.in](mailto:rokhum@che.nits.ac.in)

Received 4 October 2023; Revised 11 January 2024; Accepted 28 February 2024; Published 25 March 2024

Academic Editor: Shashi Bhatia

Copyright © 2024 Hlawancheu Zohmingliana et al. This is an open access article distributed under the Creative Commons Attribution License, which permits unrestricted use, distribution, and reproduction in any medium, provided the original work is properly cited.

*Jatropha curcas* oil (JCO) is a promising source for the manufacturing of biodiesel and has gained a lot of attention due to its environmental friendliness and availability in many parts of the world as a result of the rising need for energy. In this study, JCO was converted to biodiesel using a heterogeneous CaO-ZrO<sub>2</sub> catalyst made from biomass and MOFs. The central composite design of response surface technique was used to change the transesterification parameters to enhance JCO conversion. After optimization using RSM, the reaction parameters were set to a catalyst loading of 6.34 wt%, a reaction time of 68 minutes, a temperature of 92.9°C, and a methanol-to-oil molar ratio of 18 : 1; then, the yield of biodiesel was found to be 97.12 ± 0.4%. Using various analytical techniques, the chemical composition, texture, and its morphology have been examined by FT-IR, SEM-EDS, XRD, TGA, and BET. Moreover, <sup>1</sup>H NMR, <sup>13</sup>C NMR, and GC-MS have all been used to describe the biodiesel that has been created. While the catalyst's activity reduced, it was found that, after being washed with hexane and dried by calcination, it could still be used up to the fifth cycle.

## 1. Introduction

Our high level of life and expanding human population have caused a rise in our energy use. 80% of the energy used today comes from fossil fuels alone, with the transportation sector using 58% of this total. Because of the harm caused by the widespread use of fossil fuels, awareness has grown about alternate renewable energy sources [1]. In addition to the depletion of fossil fuel reserves, the air pollution brought on by the use of fossil fuels and global warming have prompted us to look for alternative energy sources. The manufacture of biodiesel via esterification

and transesterification using methanol and a catalyst uses renewable feedstock such as animal fats and edible and nonedible oil [2]. One of the main advantages of using biodiesel as a fuel is the low emission of CO<sub>2</sub> and its renewability and biodegradability [3]. Although edible oil accounts for 95% of the world's biodiesel output, using this resource may increase manufacturing costs [4]. Nonedible oils like *Pongamia pinnata* (also known as "Karanja oil, KO") and *Jatropha curcas* oil (JCO) have been widely employed to combat this issue [5, 6]. Due to reduced manufacturing costs and deforestation, JCO has become more popular as a feedstock [7].

Both a homogeneous catalyst and a heterogeneous catalyst have been employed to convert oil to biodiesel. Although transesterification was faster using a homogeneous catalyst, there was a significant quantity of wastewater produced during the catalyst separation and biodiesel purification steps, which increased production costs and polluted the environment [8]. The catalyst used for transesterification may be acid catalyst, base catalyst, and enzyme catalyst [9]. Homogeneous catalysts are usually used for biodiesel production from vegetable oils [10]. Because of their high activity, cheap cost, and quick reaction rate even under benign circumstances, homogeneous catalysts are particularly efficient. Nevertheless, they have a number of process issues, including the production of soap, separation during purification, and the production of a lot of wastewater during washing [4, 11]. The use of heterogeneous catalysts in the transesterification process may be able to address some of the issues with homogeneous catalyst [12]. Contrarily, heterogeneous catalysts provide a number of benefits for the process, including simplicity of separation, environmental friendliness, lack of toxicity, resistance to high temperatures, and ease of recycling [13].

CaO, MgO, and ZnO are some examples of solid heterogeneous catalysts, and CaO is one of the best candidates due to its high stability, low cost, and widespread availability [6]. CaO, however, might not be appropriate for continuous processes because of its high particle size, which presents substantial flow resistance and causes a significant pressure drop across the flow reactor [14]. In order to improve the activity of CaO, a strategy of combining with other metal oxide is commonly employed [15]. The catalytic activity of CaO is stabilized and improved by ZrO<sub>2</sub>'s unique thermal stability and high specific surface area. A larger surface area of the catalyst boosts its activity, and the pore structure controls how widely the active site is dispersed; therefore, it is preferable for the pore structure to be well-organized [16]. In one study, it was discovered that the capacity of the reactants to diffuse through the pores of the catalyst, which increases the synthesis of biodiesel, improved the rate of reaction when the catalyst's pore structure was linked by meso- and macroporous channels [17].

Metal-organic frameworks (MOF) are shown to have intrinsic properties, such as crystalline open structure, a large specific surface area, and flexible functionalities that make them a better porous material for the manufacture of solid catalysts. One of the most researched MOFs, UiO-66 (Zr<sub>6</sub>O<sub>4</sub>(OH)<sub>4</sub>), has been applied in a variety of scientific sectors [12, 18]. In this studies, the catalyst CaO-ZrO<sub>2</sub> has been derived from a reaction of CaO from snail shell and UiO-66.

The generation of biodiesel is influenced by a number of important elements. Catalyst loading, reaction temperature, reaction time, and the methanol-to-oil molar ratio (MTOR) are some of the major factors that directly affect the yield. So, optimizing these variables is essential for increasing the effectiveness of the biodiesel manufacturing process (Bahar [17]). The response surface methodology (RSM) is a potent technique for maximizing the variables in the manufacture of biodiesel. Using data from experiments, the model depicts the functional connection between a number of input factors

and one or more responses of the process [19]. It reduces the number of experimental runs by doing away with the necessity for one factor at a time (OFAT). A central composite design (CCD) of RSM was used in transesterification in one study and predicted a 99.36% output of biodiesel. Experimental measurements revealed a 98.69% biodiesel output at the conditions established by CCD [20].

In this study, we report the catalyst multifunctionality by extending use to the conversion of hardy yet inedible *Jatropha curcas* oil (JCO), and the pursuit of producing biodiesel from affordable, nonedible oil has become progressively significant due to its dual benefits of sustainability and cost-efficiency. In this context, JCO has gained attention in the energy sector, as it holds promise as a viable feedstock for biodiesel manufacturing and a renewable energy solution for numerous nations. A software-guided technique RSM-CCD method was used to optimize the reaction temperature, time, catalyst, and methanol-to-oil ratio, and under optimized reaction condition, the biodiesel yield was found to be  $97.12 \pm 0.4\%$ . The catalyst was successfully utilized for five cycles after being recovered by washing and drying.

## 2. Material and Methods

**2.1. Chemical and Material Used.** The supplier of JCO was in Delhi, India. *Pila* spp. waste snail shells were purchased in Mizoram, India. Terephthalic acid and zirconium oxychloride octahydrate were bought from Sigma-Aldrich in Bengaluru, India. Methanol (analytical grade), dimethyl formamide, and acetic acid were bought from Merck in Silchar, India. The compounds were not further purified before usage.

### 2.2. Catalyst Preparation

**2.2.1. MOF UiO-66 Preparation.** The MOF UiO-66 was prepared in accordance with the literature that is already published [21]. Benzene-1,4-dicarboxylic acid and zirconium (IV) oxychloride octahydrate were dissolved in N,N-dimethylformamide (30 mL, 99%) and agitated for 30 minutes. Glacial acetic acid (2.0 mL) and concentrated hydrochloric acid (1.5 mL, 37%) were added while being vigorously stirred. The mixture was then sealed in a 100 mL Pyrex Schott bottle and heated in an oven for two hours at 100°C. This produced a thick, white gel known as UiO-66. The 50 mL of N,N-dimethylformamide was aggressively stirred into the UiO-66 gel. After being centrifuged for 10 minutes at 4000 rpm with the diluted UiO-66 suspension (7 mL per tube), the supernatant was decanted. UiO-66 was created by further washing the gel with methanol for 10 minutes at 4000 rpm and drying it for 6 hours at 100°C in a vacuum oven.

**2.2.2. Preparation of CaO from Snail Shell.** The preprocessing procedure used was consistent with the previous research [22], in which the collected snail shells were repeatedly cleansed with distilled water to get rid of unwanted impurities and dried in an oven for 12 hours at 100°C. With a mortar and pestle, the snail shells were then reduced to a fine powder, sieved (with a mesh size of 125-250 m), and

then calcined for four hours at 900°C in a muffle furnace to produce CaO.

**2.2.3. Preparation of MOF-Based CaO-ZrO<sub>2</sub> Catalyst.** Wet impregnation method was used to make the catalyst, which included dispersing 0.5 g of UiO-66 in 30 mL of distilled water, adding a small quantity of CaO obtained from snail shells (30, 40, 50, 60, or 70 weight percent), and rapidly stirring the mixture at 30°C for 10 hours. The resulting mixture was then heated to 100°C for 16 hours with the generation of catalyst precursors. Following that, the precursor was heated to various temperatures of 600°C, 650°C, 700°C, and 750°C in a tube furnace under an inert N<sub>2</sub> environment in order to find the ideal activation temperature [12, 18].

**2.3. Characterization of Catalyst.** X-ray powder diffraction (XRD) was performed using Cu K radiation with a  $2\theta = 7-70^\circ$  angle on an XPert Pro diffractometer. 100 mA and 40kV were the operational current and voltage, respectively. Using Brunauer-Emmett-Teller (BET) analysis, the total pore volume and total surface area were determined using a Quanta Chrome Nova 2200e surface area and pore size analyzer. The temperature range for the TGA was 20–700°C, with a heating rate of 5°C min<sup>-1</sup>, and it was carried out with a continuous flow of nitrogen using a Mettler Toledo TGA/DSC. Fourier transform infrared (FT-IR) analysis was used to identify functional groups in the materials, and an IR spectrometer equipped with a 3000 Hyperion FT-IR spectrometer was used to capture IR spectra in the 400–4000 cm<sup>-1</sup> range (Bruker, Germany). Under 100 mA beam current, 30kV, and 5000x magnification on an FEI Quanta FEG 200F microscope, elemental mapping and SEM-EDS were utilized to evaluate the catalyst's morphology. Pictures from transmission electron microscopy (TEM) were captured using a JEOL JEM2100 microscope. Thermo's K-alpha XPS spectrometer and a monochromatic Al K X-ray source were used to evaluate X-ray photoelectron spectroscopy (XPS) [12, 18].

**2.4. Production of FAME by Simultaneous Esterification and Transesterification.** A catalyst loading of 0.054 g, (6 wt% w.r.t. JCO), methanol (0.64 g, 20 mmol), and JCO (0.900 g, 1 mmol) were introduced to a 20 mL reaction pressure tube. The reaction mixture was then placed in a convention heating (an oil bath equipped with magnetic stirrer with heating) containing glycerol as a heating medium and maintaining oil bath temperature constant at 90°C, kept on a magnetic stirrer, and stirred for 90 minutes at 400 rpm. When the reaction was finished, the catalyst was separated using centrifuge at 4000 rpm. Transesterification and esterification of JCO to produce biodiesel are shown in Figures 1(a) and 1(b) respectively. The experimental setup is illustrated in Supplementary Material (SM) Figure S1.

**2.5. Characterization of Biodiesel.** The reaction product was assessed using an Agilent 7890 with a FID detector for gas chromatography-high-resolution mass spectrometry (GC-HRMS) (55–230°C temperature range; 10°C per minute ramp rate). Tetramethylsilane was used as an internal standard and CDCl<sub>3</sub> as a solvent to acquire the <sup>1</sup>H and <sup>13</sup>C NMR spectra using a Bruker ASCEND-600. The JCO con-

version (C) to nonisolated FAME was calculated using <sup>1</sup>H NMR data. The integrals for methoxy and methylene groups ( $A_{Me}$  and  $A_{CH_2}$ , respectively, in Eq. (1) used to calculate conversion of soybean oil to biodiesel and yield of biodiesel was calculated using Eq. (2). According to standard American Society for Testing Materials (ASTM) techniques, the properties of the generated biodiesel were investigated. The distinctive peak of the biodiesel produced from JCO was located using Fourier transform infrared (FT-IR). The conversion of JCO to biodiesel was calculated using the ratio of the integrated areas of the methoxy protons of FAME and the -CH<sub>2</sub> protons from the <sup>1</sup>H NMR spectra. The conversion and yield of JCO to biodiesel were calculated using the following formula:

$$\text{Conversion (C)\%} = 100 \times \left( \frac{2A_{Me}}{3A_{CH_2}} \right), \quad (1)$$

where  $A_{Me}$  is the integral area portion of -OCH<sub>3</sub> and  $A_{CH_2}$  is the area of -CH<sub>2</sub>. The biodiesel yield was calculated by the following equation:

$$\text{Yield (\%)} = \frac{\text{weight of biodiesel produced}}{\text{weight of JCO used}} \times 100. \quad (2)$$

**2.6. Kinetic Study of Biodiesel.** The transesterification is assumed to follow a pseudo-first-order kinetics as alcohol is used in excess quantity to the required stoichiometric molar ratio 3:1 (alcohol to oil) [23]. To calculate activation energy, the reaction was carried out at different temperatures, viz., 50, 60, 70, 80, and 90°C. The conversion of JCO to biodiesel at different times was obtained, and apparent first-order rate constant and activation energy [24] were calculated by the following equations (3) and (4), respectively:

$$-\ln(1 - X) = kt, \quad (3)$$

$$\ln k = -\frac{E_a}{RT} + \ln P, \quad (4)$$

where  $X$  is the JCO conversion at time  $t$ ,  $T$  is the reaction temperature,  $P$  is the pre-exponential factor, and  $R$  is gas constant and is equal to  $8.314 \times 10^{-3} \text{ JK}^{-1} \text{ mol}^{-1}$ .

**2.7. Response Surface Methodology (RSM).** RSM is a method for creating, enhancing, and optimizing various key parameters of a process even when there are complicated interactions present [4]. The primary goal of RSM is to identify the region that meets the operating requirements or the process' ideal operational circumstances [25]. At five levels of independent variables ranging from -1 to +1, 30 experimental runs were carried out with four variables: temperature ( $A$ ), time ( $B$ ), methanol-to-oil ratio ( $C$ ), and catalyst loading ( $D$ ). A quadratic polynomial equation (Eq. (5))

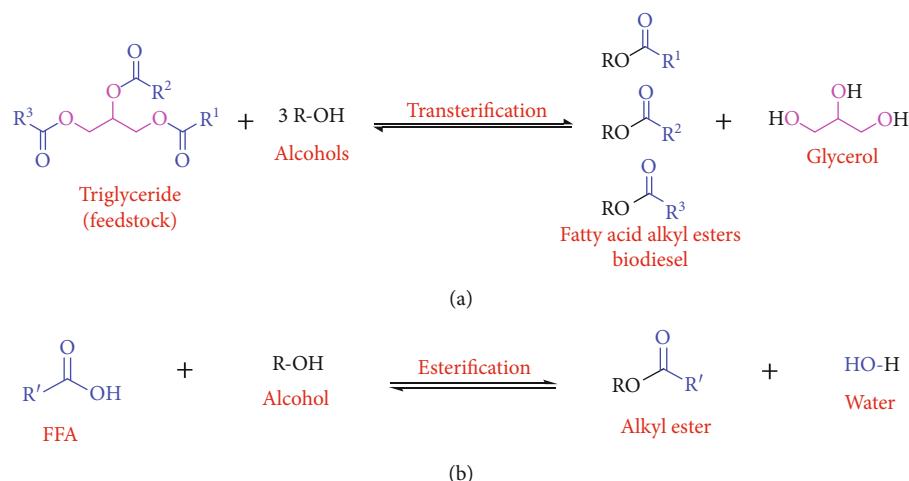


FIGURE 1: Biodiesel production via transesterification using the TGs in JCO (a). Biodiesel production using esterification of a JCO FFA content (b).

was utilized to analyze how the components performed and how their interactions impacted production efficiency (optimal response).

$$\begin{aligned} \text{Biodiesel yield}(\%) = & \alpha_0 + \alpha_1 A + \alpha_2 B + \alpha_3 C + \alpha_4 D + \alpha_{12} AB \\ & + \alpha_{13} AC + \alpha_{14} AD + \alpha_{23} BC + \alpha_{24} BD \\ & + \alpha_{34} CD + \alpha_{11} A^2 + \alpha_{22} B^2 + \alpha_{33} C^2 + \alpha_{44} D^2, \end{aligned} \quad (5)$$

where the intercept term is  $\alpha_0$ ; the coefficients of the linear terms are  $\alpha_{1-4}$ ; the coefficients of the interaction terms are  $\alpha_{12-14}$ ,  $\alpha_{23}$ ,  $\alpha_{24}$ , and  $\alpha_{34}$ ; the coefficients of the quadratic terms are  $\alpha_{11}$ ,  $\alpha_{22}$ ,  $\alpha_{33}$ , and  $\alpha_{44}$ ; and  $A$ - $D$  are the coded factors.

Analysis of variance (ANOVA) was carried out using the Design Experts 13.0 software. Fischer's test, i.e.,  $F$ -value in an ANOVA research, establishes the importance of the selected model and each parameter influencing the answer. Nevertheless, the  $p$  value provides information on the likelihood of obtaining the  $F$ -value in this range [26].

**2.8. Heterogeneity and Reusability Test for the Catalyst.** The heterogeneity of the MOF-derived CaO-ZrO<sub>2</sub> catalyst described in this study was confirmed using the hot filtering method (Sheldon's test) [27]. When reaction conditions were tuned, the solid catalyst was filtered out of the reaction mixture. The reaction was then carried out for an additional 90 minutes without the presence of a solid catalyst under otherwise identical circumstances. TLC was used to keep track of how the reaction was developing.

Consecutive batch transesterifications were used to test the synthesized catalyst's reusability. Under ideal transesterification conditions, JCO and methanol were transesterified using the pristine catalyst. After that, the isolated catalyst underwent two methanol washes to remove any organics that had adhered to it. Before being employed in the ensuing transesterification, it was then dried for a further five hours

at 80°C in a vacuum to assure activation. The fifth reaction cycle was completed by repeating this procedure.

### 3. Results and Discussion

**3.1. Catalyst Characterization.** A MOF-based CaO-ZrO<sub>2</sub> catalyst was synthesized using wet impregnation approach. The inclusion of CaO into the lattice of ZrO<sub>2</sub> is confirmed by the XRD of CaO-ZrO<sub>2</sub> as shown in Figure 2(a). The monoclinic zirconia (m-ZrO<sub>2</sub>) and tetraclinic zirconia were formed using UiO-66 as a sacrifice template (t-ZrO<sub>2</sub>). The FT-IR study (Figure 2(b)) revealed three significant CaO-ZrO<sub>2</sub> peaks, each of which corresponds to a different process, such as the stretching vibration of Ca-O and Zr-O that overlap, the creation of Ca-O-Zr, and the change from traditional m-ZrO<sub>2</sub> to t-ZrO<sub>2</sub>. TGA (Figure 2(c)) revealed that the catalyst breakdown that occurred (395-452°C), due to the decomposition of Ca(OH)<sub>2</sub>. The second stage of mass lose observed around 615°C attributed to the degradation of UiO-66 and above 750°C, the catalyst mass reduction to occur due to the formation of ZrO<sub>2</sub> and CaO. From BET analysis (Figure 2(d)), the pore volume and surface area of the catalyst were found to be 0.013 cc g<sup>-1</sup> and 7.9 m<sup>2</sup> g<sup>-1</sup>, respectively.

The SEM images in Figure 3 show that upon loading with calcium oxide on UiO-66 and activation at 650°C, a size distribution of spherical particles was generated for CaO-ZrO<sub>2</sub>, exhibiting homogeneity albeit not perfection, and from EDS analysis in Figure 3(f), Zr, O, Ca, and C were detected with weight percentages of 6.35, 32.38, 21.83, and 39.45, respectively. Additionally, SEM images and EDS of the catalyst before calcination are shown in Figure S2 (a and b) displaying long rod shape-like structure. The TEM images illustrated in Figure S2 (c and d) validated the spherical dimensions of the particles, consistent with the SEM micrograph findings.

**3.2. Analyzing Data and Modelling Outcomes with the Response Surface Method (RSM).** A second-order polynomial regression equation was developed using coded units



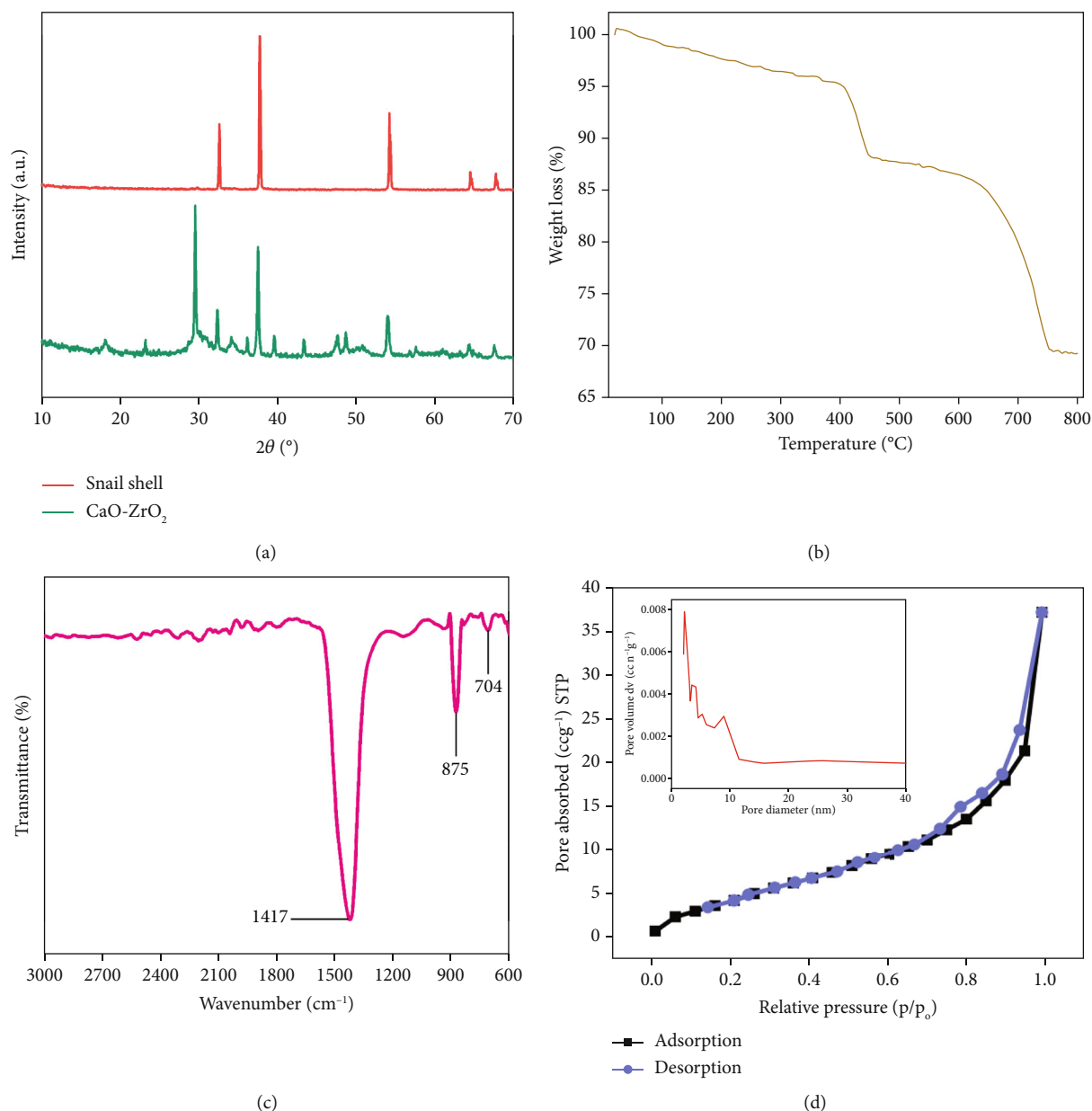


FIGURE 2: (a) XRD patterns, (b) TGA thermogram, (c) FT-IR spectra, and (d) N<sub>2</sub> adsorption-desorption isotherm and BJH pore size distribution curve (inset) of the catalyst CaO-ZrO<sub>2</sub>.

for the relationship between biodiesel yield and independent variables and is shown in Eq. (5). The results of transesterification of JCO investigated with RSM are given in Table 1.

The model equation for the biodiesel yield as a result of the coded factors for the independent variables is given as

$$\begin{aligned}
 \text{Biodiesel yield}(\%) = & 95.20 + 1.22A - 0.2542B + 2.01C + 0.8208D \\
 & - 2.92AB - 0.5312AC - 1.58AD - 1.17BC \\
 & - 0.3437BD - 0.0312CD - 3.94A^2 - 1.19B^2 \\
 & - 0.8531C^2 - 2.14D^2,
 \end{aligned}
 \tag{6}$$

where *A* is the temperature, *B* is the time, *C* is the MTOR (molar ratio), and *D* is the catalyst loading (wt%).

The significance of each coefficient in Eq. (6) is performed by analysis of variance (ANOVA). The range of real biodiesel production from laboratory trials is between 76.40 and 96.83 wt%. The regression model was significant at 95% confidence level. The value of correlation coefficient ( $R^2 = 0.9906$ ) was found to be reasonable which clearly indicates that 95% of the effect on the biodiesel yield was explained by the variance in the process variables.

In Table 2, the experimental ANOVA findings are displayed. Fischer’s statistical test (*F*-test) is part of the study; the *p* values define the likelihood that an *F*-value of any magnitude would exist, and the sum of squares establishes the importance of the parameters to the model performance [26].

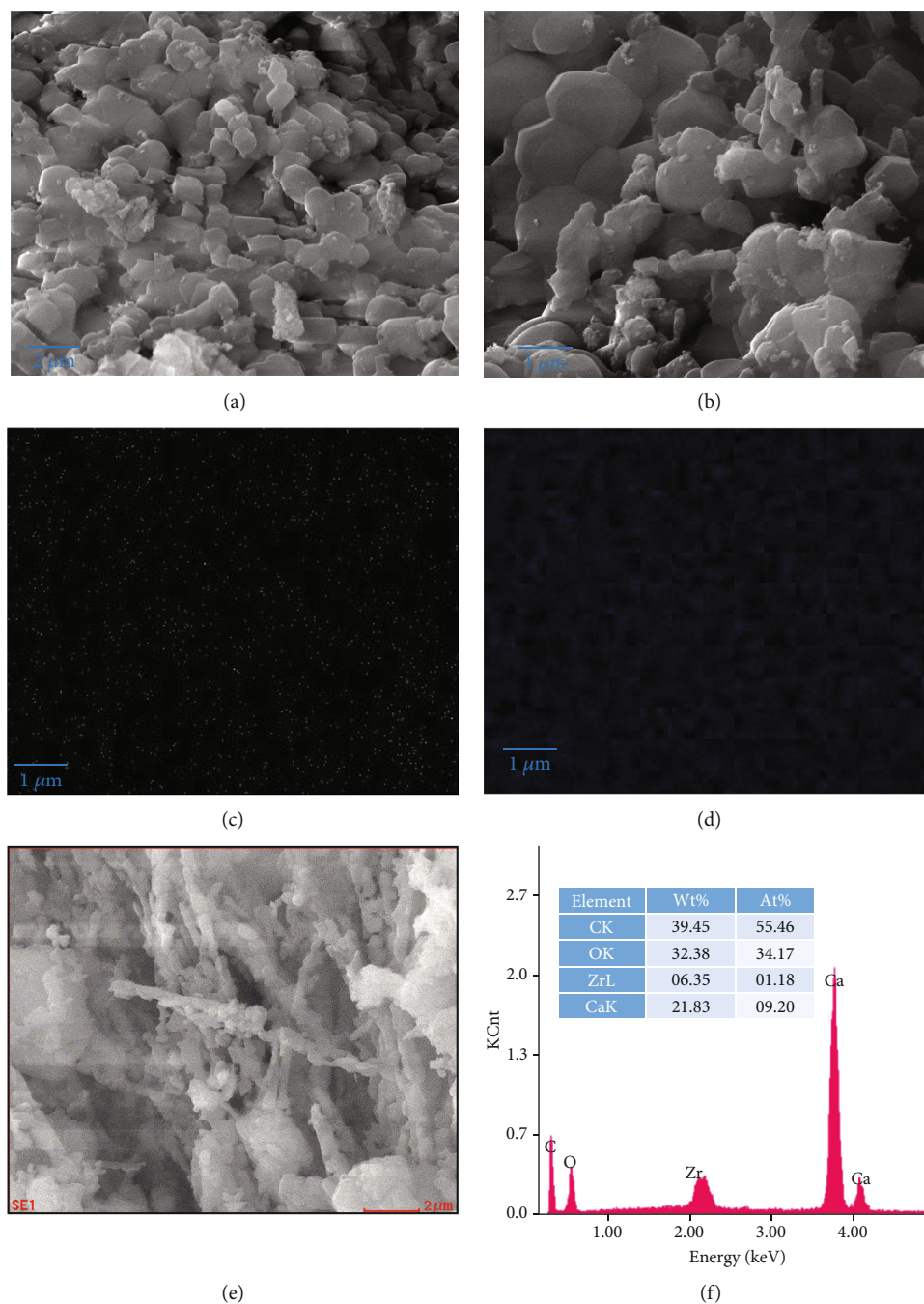


FIGURE 3: (a, b) SEM images of the fresh catalyst CaO-ZrO<sub>2</sub>. Elemental mapping of (c) Zr and (d) Ca. (f) EDS data of the area in the white box in (e).

The selected quadratic model's  $F$ -value was 112.60, which is high enough to show the model's significance. A significant  $F$ -value was demonstrated to have a 0.01% probability of being caused by noise. According to this finding, the model may be used to maximize biodiesel yield from JCO employing a CaO-ZrO<sub>2</sub> heterogeneous catalyst. A  $p$  value  $< 0.0500$  indicates that model terms are significant. In this case,  $A$ ,  $C$ ,  $D$ ,  $AB$ ,  $AD$ ,  $BC$ ,  $A^2$ ,  $B^2$ ,  $C^2$ , and  $D^2$  are significant model terms. The calculated correlation coefficient  $R^2$  of the model, which is 0.9906, may be used to

explain why the experimental data match the selected model perfectly. As measured by the signal-to-noise ratio, the model's adequate precision was judged to be 36.67, with a value larger than 4 being desired [28]. This demonstrates that the model may be utilized to explore the design space. Given that a value of 10% is preferred, the % coefficient of variance (CV) for the model was 0.8309, showing a satisfactory connection between the predicted and actual yield values.

The plot of studentized residuals against the normal distribution probability is shown in Figure 4(a). As the data

TABLE 1: Design matrix for the transesterification process with experimental variables (*A–D*) and expected and actual biodiesel production.

Std	Run	Space type	Temperature (°C) ( <i>A</i> )	Time (min) ( <i>B</i> )	MTOR ( <i>C</i> )	Catalyst loading (wt%) ( <i>D</i> )	Actual biodiesel yield (%)	Predicted biodiesel yield (%)
21	1	Axial	85	90	5	6	86.8	87.76
26	2	Center	85	90	15	6	95.2	95.2
3	3	Factorial	60	120	10	4	85.3	85.05
12	4	Factorial	110	120	10	8	83.3	83.74
24	5	Axial	85	90	15	10	88.2	88.28
8	6	Factorial	110	120	20	4	85.9	86.57
1	7	Factorial	60	60	10	4	76.4	76.7
23	8	Axial	85	90	15	2	85.1	85
2	9	Factorial	110	60	10	4	89.7	89.2
7	10	Factorial	60	120	20	4	87.5	87.87
15	11	Factorial	60	120	20	8	91.1	91.92
13	12	Factorial	60	60	20	8	89.5	89.62
28	13	Center	85	90	15	6	94.5	95.2
19	14	Axial	85	30	15	6	90.7	90.95
11	15	Factorial	60	120	10	8	89.7	89.23
5	16	Factorial	60	60	20	4	84.3	84.19
20	17	Axial	85	150	15	6	90.2	89.93
10	18	Factorial	110	60	10	8	89.1	88.43
27	19	Center	85	90	15	6	94.3	95.2
4	20	Factorial	110	120	10	4	86.3	85.88
29	21	Center	85	90	15	6	95.8	95.2
14	22	Factorial	110	60	20	8	93.1	93.67
25	23	Center	85	90	15	6	96.1	95.2
9	24	Factorial	60	60	10	8	82.6	82.25
18	25	Axial	135	90	15	6	81.7	81.88
6	26	Factorial	110	60	20	4	94.4	94.57
30	27	Center	85	90	15	6	95.3	95.2
17	28	Axial	35	90	15	6	77.2	77
16	29	Factorial	110	120	20	8	84.9	84.3
22	30	Axial	85	90	25	6	96.8	95.81

points were clearly on a straight line, it can be concluded that the residuals following studentization had a normal distribution. Inaccurate confidence intervals and  $p$  values may result in an irregular  $s$ -curve, which is deemed to be flawed for the model [29]. The predicted yield was plotted against the studentized residuals in Figure 4(b), and it was clear that the residuals were scattered randomly over the plot within the constraints of  $\pm 4$ , indicating that the initial response value is unrelated to the expected value. It also indicates that the model is adequate and suitable. The residual vs. experimental runs are shown in Figure 4(c). A large residual may arise due to the presence of noise in the experiment. This may lead to difference in the actual and predicted values. All residuals fell within the  $\pm 4.0$  range, demonstrating that there was no detectable data error and that the fitted model properly reflected all of the data [30]. Figure 4(d) shows a plot of the actual and anticipated biodiesel yield. The model may be used to fore-

cast the maximum biodiesel production since the value is near to the straight line and is therefore appropriate for the actual data.

The perturbation plot in Figure S3 describes how all the parameters affect the conversion of JCO to biodiesel while keeping other factors constant at their center values. The steepness of the plot describes how the change in the variables affects the production of biodiesel. As a result, we may infer from the perturbation plot that *A* is the dominating component between the lower level (-1) and the middle level (0) since it deviates from the reference point the most. *C*, *D*, and *B* are therefore the next three prominent factors. On the other hand, the variable *C* dominates from the intermediate level (level 0) to the higher level (level +1), followed by *A*, *B*, and *D*. We can infer from the perturbation plot that the variable *A*, or temperature, has the most dominant effect up until the middle level (0) as we increase each of the different

TABLE 2: Results of the statistical analysis for the JCO transesterification regression model.

Source	Sum of squares	df	Mean square	F-value	p value	Remarks
Model	856.23	14	61.16	112.6	<0.0001	Significant
A—temp	35.77	1	35.77	65.86	<0.0001	
B—time	1.55	1	1.55	2.85	0.1118	
C—MTOR	97.2	1	97.2	178.96	<0.0001	
D—CL	16.17	1	16.17	29.77	<0.0001	
AB	136.31	1	136.31	250.95	<0.0001	
AC	4.52	1	4.52	8.31	0.0114	
AD	40.01	1	40.01	73.65	<0.0001	
BC	21.86	1	21.86	40.24	<0.0001	
BD	1.89	1	1.89	3.48	0.0818	
CD	0.0156	1	0.0156	0.0288	0.8676	
A <sup>2</sup>	425.93	1	425.93	784.15	<0.0001	
B <sup>2</sup>	38.88	1	38.88	71.58	<0.0001	
C <sup>2</sup>	19.96	1	19.96	36.75	<0.0001	
D <sup>2</sup>	125.69	1	125.69	231.39	<0.0001	
Residual	8.15	15	0.5432			
Lack of fit	5.67	10	0.5667	1.14	0.4691	Not significant
Pure error	2.48	5	0.496			
Cor total	864.38	29				

variables, but once they reach the middle level (0), the increase of variable C, or MTOR, has a significant impact on the biodiesel product, while the other variables show a decrease in the product. Based on the general steepness of the slope and the ANOVA analysis, it can be concluded that A and C have a significant influence on the biodiesel yield.

**3.2.1. Interaction of Input Variables.** Using a surface model plot, the effects of the four independent variables (time, temperature, catalyst loading (CL), and MTOR) on the generation of biodiesel were investigated. Two variables' effects were looked at in various ways, while the other two variables remained constant at their midpoint levels. The interplay of temperature and reaction time is depicted in Figure 5(a), with a maximum biodiesel output occurring at 85°C and 90 min. Initially, a rise in temperature was accompanied by an increase in conversion because esterification and transesterification are both endothermic processes [7]. Both variables exhibit meaningful interaction.

Figure 5(b) shows the effect of MTOR and temperature interaction on JCO conversion. The maximum conversion of JCO from these two factors is reached when the temperature is 85°C and MTOR is 15:1. On further increase in the temperature, the biodiesel yield starts declining, while increasing MTOR increases the product. Since too much methanol dilutes the reaction mixture and lessens reactant-catalyst active-site collisions, too much MTOR also causes a slight drop [31] [32]. The 3D response curve shows that this reaction significantly depends on the interplay between temperature and MTOR.

Temperature and catalyst loading relationship is depicted in Figure 5(c). The JCO conversion was greatest at 6 wt% and 85°C, respectively. Due to the fact that both esterification and transesterification are endothermic processes, a rise in temperature originally resulted in a higher conversion rate. After a maximum conversion was reached at 6 wt%, with the further increase in the catalyst loading, there is a slight decrease in the conversion yield. A rise in the reaction mixture's viscosity that limits mass transfer may be the cause of the drop in yield brought on by the increased catalyst loading [33]. The 3D response curve demonstrated the importance of the relationship between catalyst loading and reaction temperature.

Figure 5(d) describes the interaction of time and MTOR. The model shows that MTOR shows significant changes, while the variation in time does not show a significant effect. The maximum conversion from these two variables is reached when the time of reaction is 90 min and MTOR is 15:1. Although an increase in the product is seen with further increase in MTOR, a further increase in time more than 90 min shows a slight decrease in the product [34].

The relationship between time and catalyst loading is seen in Figure 5(e). The 90-minute mark and a 6 wt% catalyst addition yielded the highest conversion. The product somewhat declines when both factors are raised more. Since transesterification is reversible, there is once again a minor drop when the reaction time is too lengthy [33].

The greatest FAME conversion rates are 15:1 and 6 wt%, respectively, in Figure 5(f), which shows how MTOR and catalyst loading interact. Due to the transesterification process' reversibility, there was a minor drop when the reaction



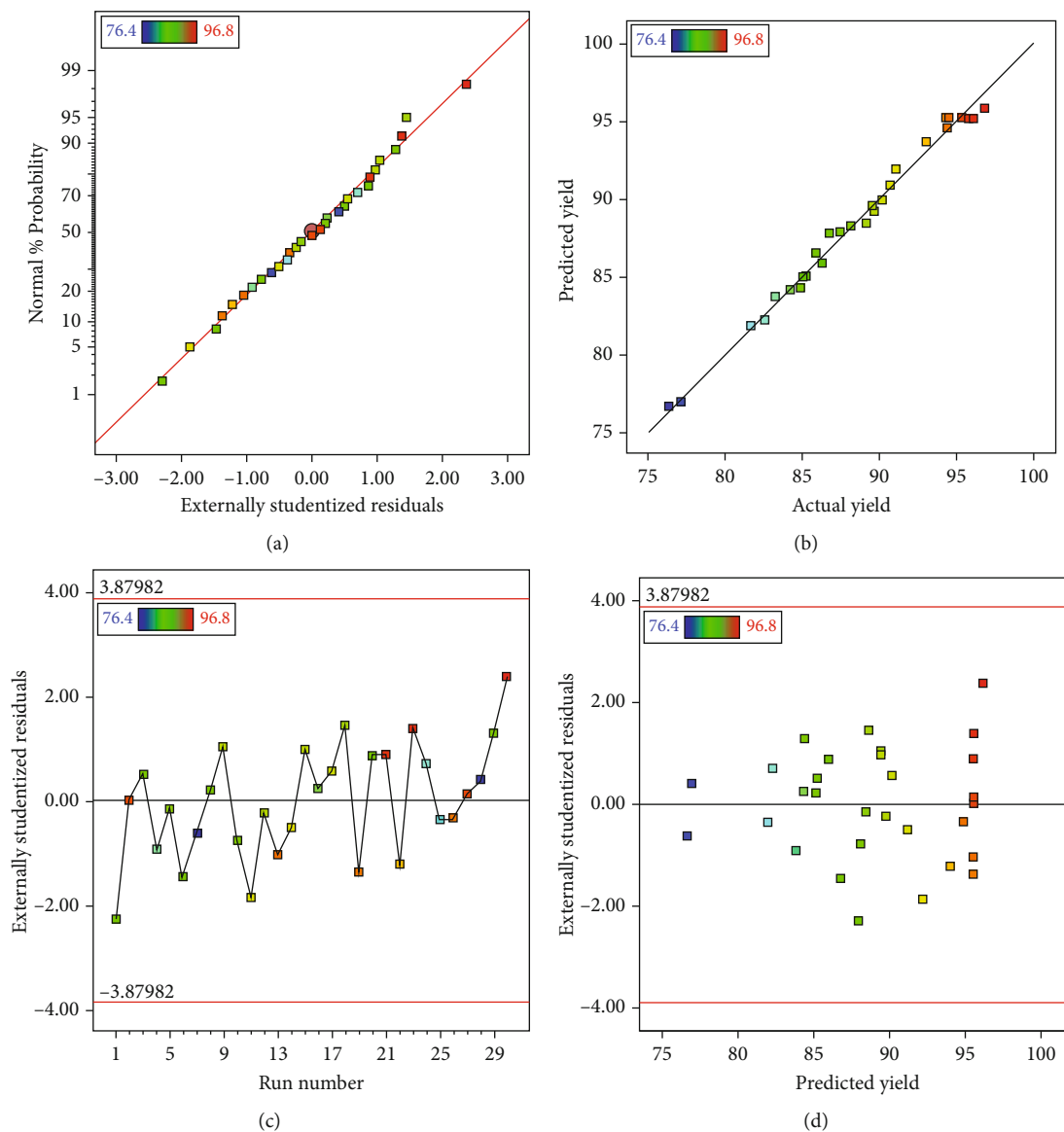


FIGURE 4: Diagnostic plots: (a) normal plot of residuals and (b) predicted vs. actual biodiesel yield. (c) Run number vs. studentized residuals and (d) studentized residuals vs. predicted biodiesel yield.

time was too lengthy [35]. Once more, the 3D response curve shows that the reaction's importance is greatly influenced by the interplay between MTOR and catalyst loading.

**3.2.2. Optimization of Biodiesel Yield.** In this work, a numerical optimization strategy was used to identify the four input variables with the best circumstances and a desirability function of 1. The optimization strategy's objective was to maximize biodiesel output while staying within the lower and higher boundaries of the variable ranges used in the study. The lower bound and upper bound of the variable are 60–110°C for temperature, 60–120 min for time, 4–8 wt% for catalyst, and 10–20 for MTOR. RSM determines the optimal condition within the selected range of variables since it is a local optimizing approach. The RSM-CCD approach's ideal conditions for the transesterification of JCO were a reaction temperature of 92.91°C, a reaction time of 68.10 min, an

MTOR of 18.28, and a CL of 6.34 wt% under the traditional technique, with a biodiesel yield of 97.87 wt%. This circumstance was used to carry out laboratory experiments in triplicate, with an average biodiesel production of  $97.12 \pm 0.4$  wt% proving the efficacy of the regression model developed in explaining the transesterification process.

**3.3. Biodiesel Characterization.** The JCO feedstock has a significant impact on the characterization of the product biodiesel, and as the crude JCO varies from location to location, the characterization is crucial in this area to determine the precise state of the product [36].  $^1\text{H}$  NMR spectroscopy on the synthesized product showed a singlet at  $\delta$  3.62 ppm corresponding to the methoxy group, confirming the successful formation of FAME. The peaks at  $\delta$  2.26 ppm correspond to the  $\alpha$ -methylene group of JCO as well as transesterified and esterified derivatives as shown in Figure 6(a).

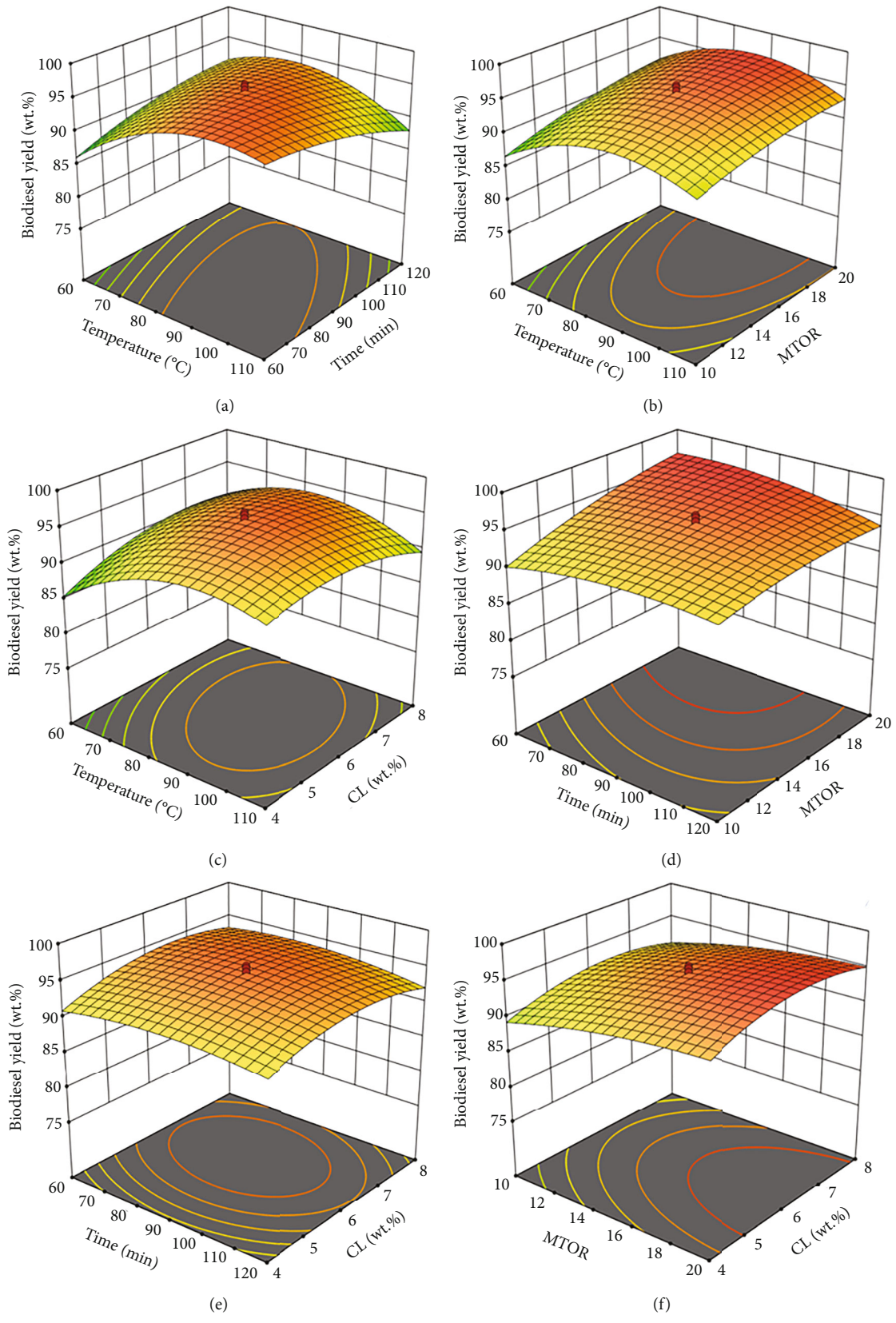
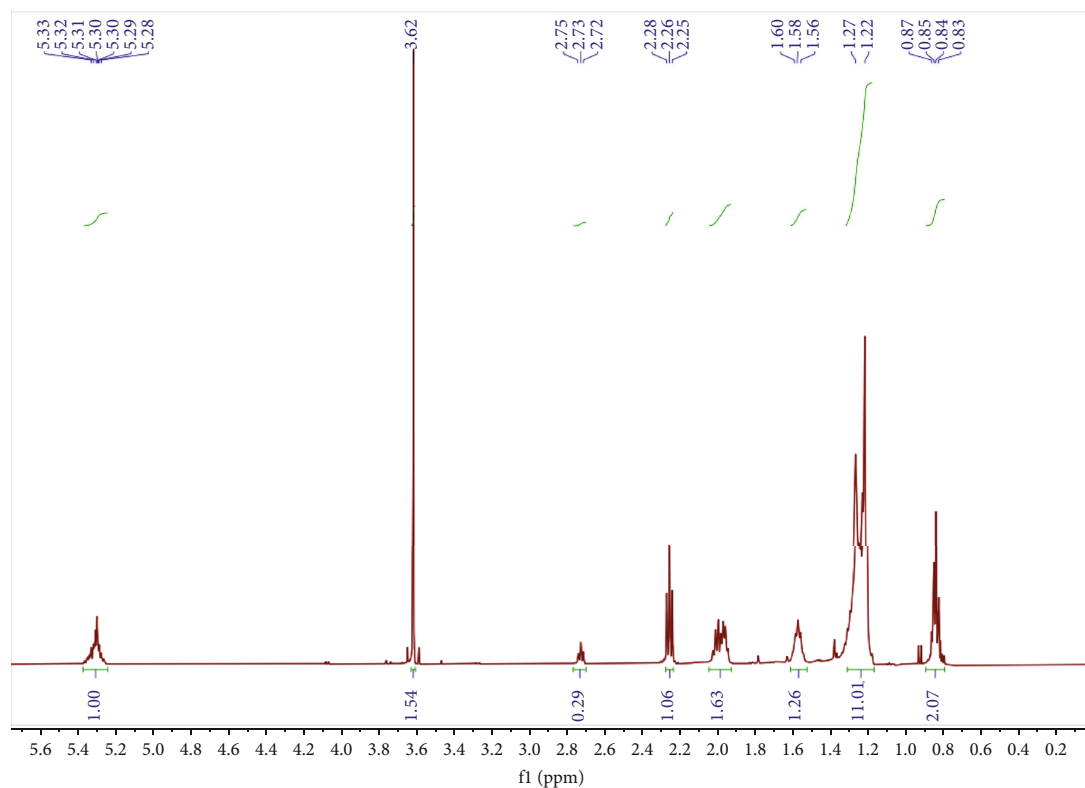
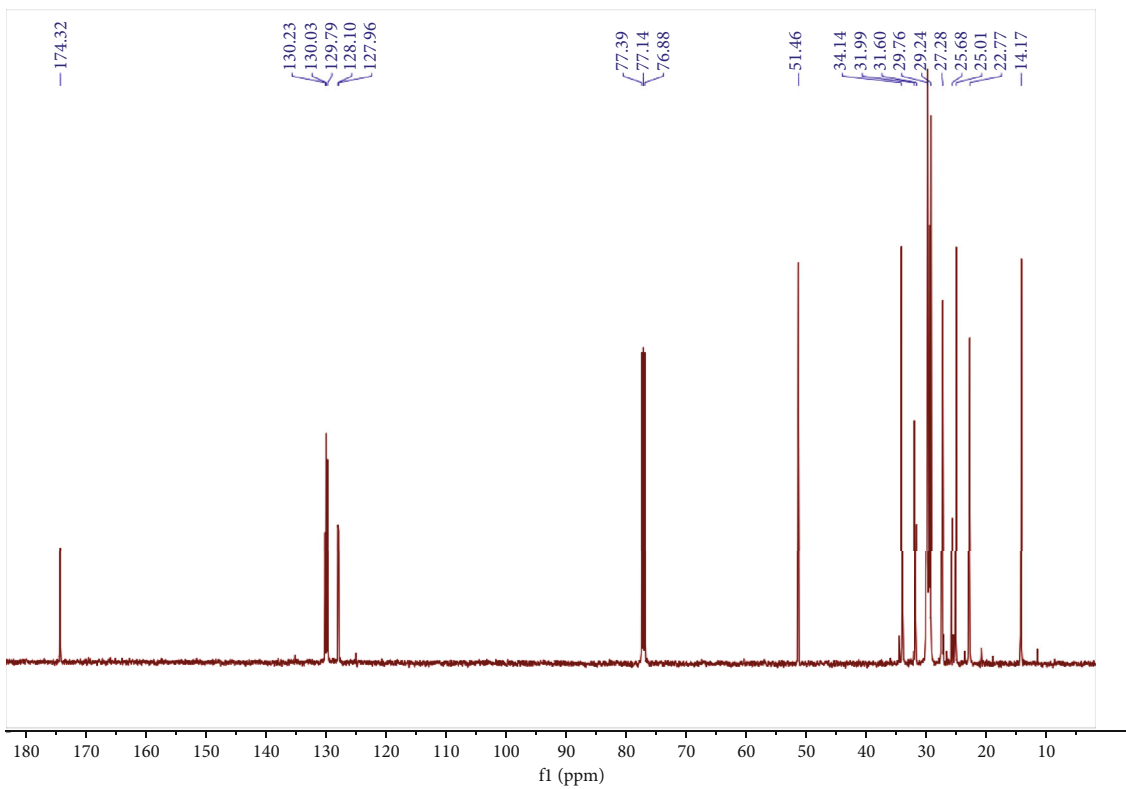


FIGURE 5: (a–f) 3D surface plot of biodiesel yield with respect to time, temperature, MTOR, and CL.



(a)



(b)

FIGURE 6: (a)  $^1\text{H}$  NMR and (b)  $^{13}\text{C}$  NMR of synthesized biodiesel.

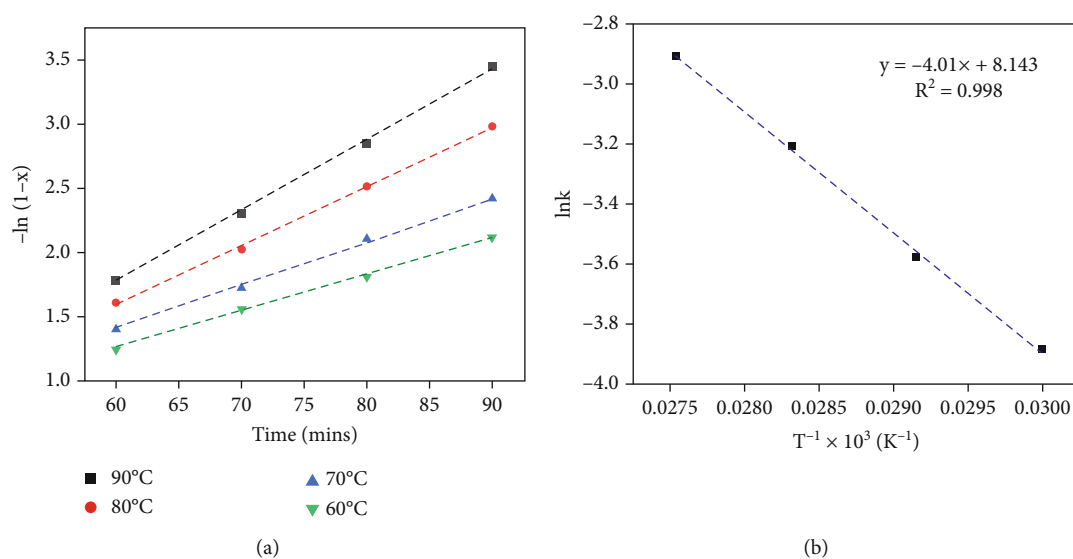
TABLE 3: Chemical composition of JCO biodiesel.

Peak no.	Component name	Retention time (min)	Corresponding acid	Proportion (%)
1	9-Hexadecenoic acid, methyl ester	12.478	C 17:1	2.20
2	Hexadecanoic acid, methyl ester	12.613	C 17:0	21.26
3	n-Propyl 9,12-octadecadienoate	13.750	C 21:2	30.40
4	9-Octadecenoic acid, methyl ester	13.788	C 19:1	32.50
5	Methyl stearate	13.909	C 19:0	11.83
6	9,12-Octadecadienoic acid, methyl ester	14.291	C 19:2	1.81

TABLE 4: The physical and chemical characteristics of the biodiesel generated in this study as determined by ASTM standards.

Property	JCO biodiesel <sup>a</sup>	ASTM limits	Testing methods
Acid value (mg KOH g <sup>-1</sup> )	0.21	<0.79	D 664
Density (g cm <sup>-3</sup> )	0.86	0.86-0.90	D 1448-1972
Flash point (°C)	145	>93	D 7215
Kinematic viscosity (cSt) <sup>b</sup>	4.33	1.90-6.00	D 445
Pour point (°C)	3.35	-15 to +6	D 97
Cetane number	56	≥47	D 6890
Cloud point (°C)	1	-3 to +12	D 2500

<sup>a</sup>This work. <sup>b</sup>At 40°C.

FIGURE 7: (a)  $-\ln(1-X)$  vs. time ( $X$  is the JCO biodiesel yield) and the relevant plot of (b)  $\ln k$  vs.  $1/T$ .

The ratio of the integrated areas of the peaks at 3.62 ppm and 2.26 ppm using Eq. (1) was used to calculate the percentage conversion from JCO to FAMEs, which was found to be 98.87%. The effective synthesis of FAMEs was also confirmed by the appearance of methoxy and carbonyl peaks at 51.46 and 174.32 ppm, respectively, in <sup>13</sup>C NMR data as shown in Figure 6(b). The corresponding numerical spectroscopic data for the synthesized biodiesel from JCO are as follows: <sup>1</sup>H NMR (500 MHz, CDCl<sub>3</sub>, 27°C):  $\delta$  5.38–5.24 (m, 2H), 3.62 (s, 3H), 2.73 (t, Hz, 2H), 2.26 (t, 2H), 2.05–1.94 (m, 6H), 1.62–1.53 (m, 1H), 1.24 (d, 8H), and 0.90–0.80

(m, 4H) and <sup>13</sup>C NMR (126 MHz, CDCl<sub>3</sub>, 27°C):  $\delta$  174.32, 129.76, 77.14, 51.46, 29.24, and 14.17.

The GC-MS analysis of the synthesized biodiesel and methyl esters that appear on the total ion chromatogram is shown in Figure S4, and the chemical composition with respect to retention time, corresponding methyl esters, and proportion is shown in Table 3. The major constituents were 9-octadecenoic acid, methyl ester (32.50%), n-propyl 9,12-octadecadienoate (30.40%), hexadecanoic acid, methyl ester (21.26%), and methyl stearate (11.83%). The measurements of the physicochemical characteristics, such as



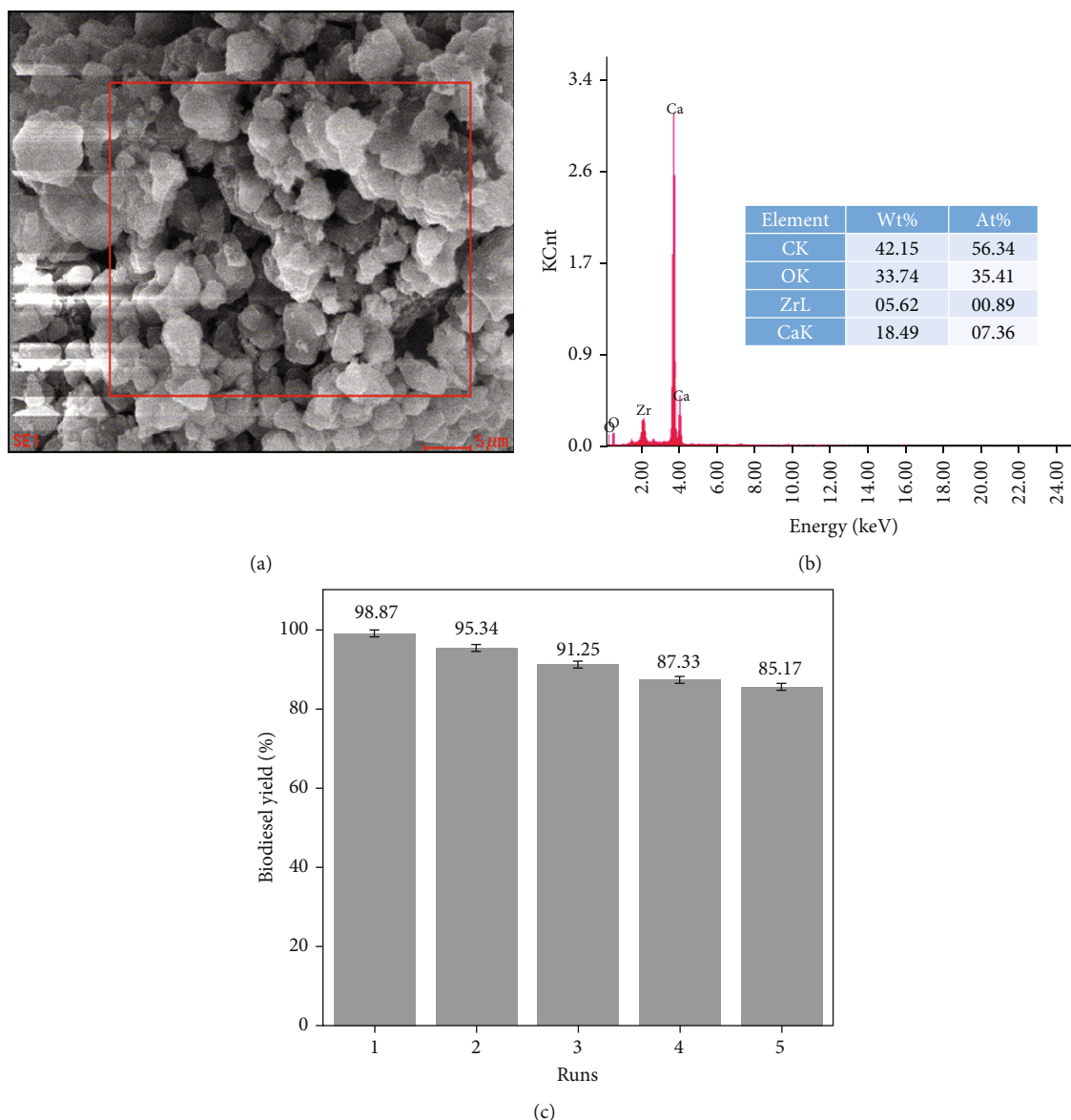


FIGURE 8: (a) SEM images of the recovered catalyst after five transesterification cycles. (b) EDS data of the area in the red box in (c). Reusability of CaO-ZrO<sub>2</sub> catalyst in the transesterification of JCO over 5 cycles.

flash point, acid value kinematic viscosity, density, and calorific value, were made. The results are all in accordance with the standards set by the American Society for Testing and Materials (ASTM) (Table 4), demonstrating the viability of using biodiesel as an alternative to petroleum-based fuels in motor vehicles. The ASTM standards are instrumental in the evaluation and assessment of the physical, mechanical, rheological, thermal, and chemical properties of crude oils, lubricating grease, automobile and aviation gasoline, hydrocarbons, and other naturally occurring energy resources used for various industrial applications. These standards enable industries, including petroleum refineries and automotive companies, to evaluate fuel composition, purity, density, miscibility, compatibility, toxicity, and thermal stability. This ensures the quality of fuel oils for safe and efficient industrial use.

**3.4. Kinetic Study of Transesterification.** A plot of  $-\ln(1-X)$  versus time for the reaction at 60–110°C is shown in Figure 7(a), which confirms that the transesterification proceeded through an expected pseudo-first-order kinetics [37]. The activation energy  $E_a$  was then calculated by fitting the rate constant to the Arrhenius equation. The slope ( $-E_a/R$ ) and intercept of the  $\ln k$  vs.  $T^{-1}$  plot confirmed pseudo-first-order kinetics. From Figure 7(b),  $E_a$  was calculated to be 33.33 kJ mol<sup>-1</sup> and the pre-exponential factor was calculated to be  $3.4 \times 10^3$  min<sup>-1</sup>.

**3.5. Catalyst Reusability.** Reusable catalysts are essential in order to save money on the reaction's total cost by reusing the original catalyst rather than purchasing a new one. Although CaO-ZrO<sub>2</sub> has been used in the manufacture of biodiesel from soybean oil and has been reported to be

TABLE 5: Comparison of the present CaO-ZrO<sub>2</sub> catalyst for the conversion of JCO to FAME with previously reported solid acid catalysts.

Entry	Catalyst	Conditions <sup>a</sup>	TOF <sup>b</sup> (mol g <sup>-1</sup> h <sup>-1</sup> )	FFA <sup>c</sup> content (wt%)	Biodiesel yield (%)	Ref.
1.	KSF clay and Amberlyst 15	12 : 1, 5, 160, 6	0.0025	6.5	70	[38]
2.	CaLaO	21 : 1, 1, 240, 10 <sup>d</sup>	0.6458	NA <sup>e</sup>	93	[3]
3.	MPD-SO <sub>3</sub> H-IL <sup>f</sup>	50 : 1, 6, 160, 8	0.0022	8	94	[32]
4.	ZrO <sub>2</sub> -Al <sub>2</sub> O <sub>3</sub>	9 : 1, 7.61, 150, 4	0.0032	NA	90.32	[39, 40]
5.	CaSO <sub>4</sub> /Fe <sub>2</sub> O <sub>3</sub> -SiO <sub>2</sub>	9 : 1, 12, 120, 4	0.0022	NA	94	[41]
6.	SO <sub>4</sub> <sup>2-</sup> /ZrO <sub>2</sub> @Al <sub>2</sub> O <sub>3</sub>	8 : 1, 8, 150, 3	0.0036	NA	78.3	[40]
7.	SO <sub>4</sub> <sup>2-</sup> /SnO <sub>2</sub> -SiO <sub>2</sub>	15 : 1, 3, 180, 2	0.0179	8.14	97	[42]
8.	AC-600- SO <sub>3</sub> H@Fe/C <sup>g</sup>	25 : 1, 10, 200, 5	0.0020	8.64	90.5	[43]
9.	Zn8@FeC <sub>400</sub>	40 : 1, 7, 160, 4	0.0038	6.43	98	[45]
10.	C-SO <sub>3</sub> H@Fe/JH <sup>h</sup>	12 : 1, 10, 80, 1.5	0.0072	NA	96.7	[45]
11.	MgZnAlO	11 : 1, 8, 182, 6	0.0021	NA	94	[46]
12.	CaO-ZrO <sub>2</sub>	20 : 1, 6, 90, 1.5	0.0118	7.84	97.12	Present work

<sup>a</sup>MeOH : JCO molar ratio, catalyst loading (wt%), temperature (°C), and time (h). <sup>b</sup>Turnover frequency. <sup>c</sup>Free fatty acid. <sup>d</sup>Minutes. <sup>e</sup>Not available. <sup>f</sup>MPD-SO<sub>3</sub>H-IL: mesoporous polymer-sulfonic acid-ionic liquid. <sup>g</sup>AC: activated carbon. <sup>h</sup>JH: Jatropha hull.

reusable, this study looked at CaO-ZrO<sub>2</sub> reusability after being used in the production of biodiesel from JCO. The catalyst was separated and recovered from the reaction mixture using filtering and then washed with hexanol before being dried in the oven for five hours at 70°C. At 500°C, calcining was used to further activate the catalyst. The catalyst was employed in five subsequent reactions in this manner, each using the identical recovery technique and improved reaction conditions (Figure 8(c)). After five catalytic transesterification reactions, the employed catalyst's SEM-EDS was examined, and SEM analysis revealed that the morphology of the catalyst remains unchanged (Figure 8(a)) whereas EDS analysis (Figure 8(b)) revealed a reduction in the quantity of zirconium and calcium ions compared with the fresh catalyst we have reported earlier [12, 18]. Deactivation is mostly brought on by metal ion leaching and active-site obstruction.

**3.6. Comparing CaO-ZrO<sub>2</sub> Catalyst with Previously Reported Catalysts.** Table 5 compares the existing CaO-ZrO<sub>2</sub> with a number of heterogeneous solid acid catalysts specifically for the conversion of JCO to FAMES. The table below provides a summary of several information, including the kind of feedstock, catalyst, turnover frequency (TOF), operational parameters, and biodiesel production. The current catalyst has numerous benefits over the other catalysts on the table for the manufacture of biodiesel from JCO. Although the biodiesel yield is not the highest among the catalyst shown in the table, those having high yield like entries 7 and 9 have a high reaction temperature and longer reaction time. The TOF of the current catalyst is higher as compared to most of the other catalyst from the entries which confirm the activity of the catalyst. Despite having high TOF by the catalyst CaLaO, the biodiesel yield is lower than the present catalyst.

## 4. Conclusion

In this study, the catalyst CaO-ZrO<sub>2</sub> has been employed successfully for the traditional technique of producing biodiesel from JCO. As anticipated by the RSM numerical optimiza-

tion process using the standard technique, the catalyst in this study exhibits outstanding activity for the transesterification of JCO, with a conversion rate of  $98.87 \pm 0.6$  and a yield of  $97.12 \pm 0.4\%$  under optimum conditions. The major constituents of the biodiesel product from JCO are 9-octadecenoic acid methyl ester, n-propyl 9,12-octadecadienoate, and hexadecanoic acid methyl ester. The RSM-CCD approach-based optimization procedure was effective in determining the optimal temperature, time, and catalyst loading for raising the biodiesel production. Moreover, the catalyst can be recycled after washing and drying with an effective yield of  $85.17 \pm 0.5\%$  up to the fifth cycle. More extensive efforts are currently being made in our laboratories to further mitigate the loss of catalyst performance.

## Abbreviations

MTOR:	Methanol-to-oil ratio
CCD:	Central composite design
JCO:	<i>Jatropha curcas</i> oil
ANOVA:	Analysis of variance
TG:	Triglyceride
RSM:	Response surface methodology
SEM:	Scanning electron microscopy
FAMES:	Fatty acid methyl esters
TGA:	Thermogravimetric analysis
FT-IR:	Fourier transform infrared spectroscopy
MOF:	Metal-organic framework
OFAT:	One factor at a time
SM:	Supplementary material
TOF:	Turnover frequency
TEM:	Transmission electron microscopy
BET:	Brunauer-Emmett-Teller
EDS:	Energy-dispersive X-ray spectroscopy
XRD:	X-ray powder diffraction
XPS:	X-ray photoelectron spectroscopy
NMR:	Nuclear magnetic resonance
GC-MS:	Gas chromatography mass spectrometry
FFA:	Free fatty acid

ASTM: American society for testing materials  
 KO: Karanja oil  
 CV: Coefficient of variance  
 CL: Catalyst loading.

## Data Availability

Data will be made available on request.

## Conflicts of Interest

The authors declare that they have no known competing financial interests or personal relationships that could have appeared to influence the work reported in this paper.

## Supplementary Materials

Supplementary material to this article can be found online. It contains the experimental setup for biodiesel production in Figure S1, SEM and EDS images of the catalyst before calcination and TEM images of the catalyst in Figure S2, the perturbation plot showing variables with a substantial impact on biodiesel yield in Figure S3, and GC-MS of synthesized biodiesel in Figure S4. (*Supplementary Materials*)

## References

- [1] S. K. Sahoo, "Renewable and sustainable energy reviews solar photovoltaic energy progress in India: a review," *Renewable and Sustainable Energy Reviews*, vol. 59, pp. 927–939, 2016.
- [2] A. Reddy, S. Aa, M. S. Islam, and S. Hamdan, "Active heterogeneous CaO catalyst synthesis from *Anadara granosa* (Kerang) seashells for *Jatropha* biodiesel production," *MATEC Web of Conferences*, vol. 87, article 02008, 2017.
- [3] S. H. Teo, M. Goto, and Y. H. Taufiq-Yap, "Biodiesel production from *Jatropha curcas* L. oil with Ca and La mixed oxide catalyst in near supercritical methanol conditions," *Journal of Supercritical Fluids*, vol. 104, pp. 243–250, 2015.
- [4] J. V. L. Ruatpuia, B. Changmai, A. Pathak et al., "Green biodiesel production from *Jatropha curcas* oil using a carbon-based solid acid catalyst: a process optimization study," *Renewable Energy*, vol. 206, pp. 597–608, 2023.
- [5] K. T. T. Amesho, Y. C. Lin, C. E. Chen, P. C. Cheng, and S. Shangdiar, "Kinetics studies of sustainable biodiesel synthesis from *Jatropha curcas* oil by exploiting bio-waste derived CaO-based heterogeneous catalyst via microwave heating system as a green chemistry technique," *Fuel*, vol. 323, article 123876, 2022.
- [6] K. T. T. Amesho, Y. C. Lin, C. E. Chen, P. C. Cheng, and V. K. Ponnusamy, "Optimization and kinetics studies of biodiesel synthesis from *Jatropha curcas* oil under the application of eco-friendly microwave heating technique: an environmentally benign and sustainable bio-waste management approach," *Sustainable Environment Research*, vol. 32, no. 1, 2022.
- [7] I. B. Laskar, B. Changmai, R. Gupta et al., "A mesoporous poly-sulfonic acid-formaldehyde polymeric catalyst for biodiesel production from *Jatropha curcas* oil," *Renewable Energy*, vol. 173, pp. 415–421, 2021.
- [8] S. Xia, X. Guo, D. Mao, Z. Shi, G. Wu, and L. Guanzhong, "Biodiesel synthesis over the CaO–ZrO<sub>2</sub> solid base catalyst prepared by a urea–nitrate combustion method," *RSC Advances*, vol. 4, no. 93, pp. 51688–51695, 2014.
- [9] J. G. Duarte, K. Leone-Ignacio, J. A. C. da Silva, R. Fernandez-Lafuente, and D. M. G. Freire, "Rapid determination of the synthetic activity of lipases/esterases via transesterification and esterification zymography," *Fuel*, vol. 177, pp. 123–129, 2016.
- [10] L. C. Meher, D. Vidya Sagar, and S. N. Naik, "Technical aspects of biodiesel production by transesterification—a review," *Renewable and Sustainable Energy Reviews*, vol. 10, no. 3, pp. 248–268, 2006.
- [11] J. V. L. Ruatpuia, G. Halder, S. Mohan et al., "Microwave-assisted biodiesel production using ZIF-8 MOF-derived nanocatalyst: a process optimization, kinetics, thermodynamics and life cycle cost analysis," *Energy Conversion and Management*, vol. 292, article 117418, 2023.
- [12] S. P. Gouda, A. Dhakshinamoorthy, and S. L. Rokhum, "Metal-organic framework as a heterogeneous catalyst for biodiesel production: a review," *Chemical Engineering Journal Advances*, vol. 12, article 100415, 2022.
- [13] J. Nisar, R. Razaq, M. Farooq et al., "Enhanced biodiesel production from *Jatropha* oil using calcined waste animal bones as catalyst," *Renewable Energy*, vol. 101, pp. 111–119, 2017.
- [14] W. Woranuch, K. Ngaosuwana, W. Kiatkittipong et al., "Fine-tuned fabrication parameters of CaO catalyst pellets for transesterification of palm oil to biodiesel," *Fuel*, vol. 323, article 124356, 2022.
- [15] Y. L. Meng, B. Y. Wang, S. F. Li, S. J. Tian, and M. H. Zhang, "Effect of calcination temperature on the activity of solid Ca/Al composite oxide-based alkaline catalyst for biodiesel production," *Bioresource Technology*, vol. 128, pp. 305–309, 2013.
- [16] H. Li, Y. Wang, X. Ma et al., "Synthesis of CaO/ZrO<sub>2</sub> based catalyst by using UiO-66(Zr) and calcium acetate for biodiesel production," *Renewable Energy*, vol. 185, pp. 970–977, 2022.
- [17] B. Laskar, T. D. Iqbal, A. Biswas et al., "Utilization of biowaste-derived catalysts for biodiesel production: process optimization using response surface methodology and particle swarm optimization method," *Energy Advances*, vol. 1, no. 5, pp. 287–302, 2022.
- [18] S. P. Gouda, A. J. Momo, P. Kumar, A. Dhakshinamoorthy, U. Rashid, and S. L. Rokhum, "Microwave-assisted biodiesel production using UiO-66 MOF derived nanocatalyst: process optimization using response surface methodology," *Catalysts*, vol. 12, no. 11, p. 1312, 2022.
- [19] J. V. L. Ruatpuia, G. Halder, D. Shi, S. Halder, and S. Lalthazuala, "comparative life cycle cost analysis of biovalorized magnetite nanocatalyst for biodiesel production: modeling, optimization, kinetics and thermodynamic study," *Bioresource Technology*, vol. 393, article 130160, 2024.
- [20] M. Balajii and S. Niju, "Banana peduncle – a green and renewable heterogeneous base catalyst for biodiesel production from *Ceiba pentandra* oil," *Renewable Energy*, vol. 146, pp. 2255–2269, 2020.
- [21] B. M. Connolly, M. Aragones-Anglada, J. Gandara-Loe et al., "Tuning porosity in macroscopic monolithic metal-organic frameworks for exceptional natural gas storage," *Nature Communications*, vol. 10, no. 1, p. 2345, 2019.
- [22] I. B. Laskar, K. Rajkumari, R. Gupta, S. Chatterjee, B. Paul, and L. Rokhum, "Waste snail shell derived heterogeneous catalyst for biodiesel production by the transesterification of soybean oil," *RSC Advances*, vol. 8, no. 36, pp. 20131–20142, 2018.

- [23] N. Kaur and A. Ali, "Kinetics and reusability of Zr/CaO as heterogeneous catalyst for the ethanolysis and methanolysis of *Jatropha curcas* oil," *Fuel Processing Technology*, vol. 119, pp. 173–184, 2014.
- [24] A. Birla, S. Bhaskar, S. N. Upadhyay, and Y. C. Sharma, "Kinetics studies of synthesis of biodiesel from waste frying oil using a heterogeneous catalyst derived from snail shell," *Bioresource Technology*, vol. 106, pp. 95–100, 2012.
- [25] U. K. Garg, M. P. Kaur, V. K. Garg, and D. Sud, "Removal of nickel (II) from aqueous solution by adsorption on agricultural waste biomass using a response surface methodological approach," *Bioresource Technology*, vol. 99, no. 5, pp. 1325–1331, 2008.
- [26] S. H. Dhawane, T. Kumar, and G. Halder, "Parametric effects and optimization on synthesis of iron (II) doped carbonaceous catalyst for the production of biodiesel," *Energy Conversion and Management*, vol. 122, pp. 310–320, 2016.
- [27] H. E. B. Lempers and R. A. Sheldon, "The stability of chromium in CrAPO-5, CrAPO-11, and CrS-1 during liquid phase oxidations," *Journal of Catalysis*, vol. 175, no. 1, pp. 62–69, 1998.
- [28] E. Betiku, A. O. Etim, O. Perea, and T. V. Ojumu, "Two-step conversion of neem (*Azadirachta indica*) seed oil into fatty methyl esters using a heterogeneous biomass-based catalyst: an example of cocoa pod husk," *Energy and Fuels*, vol. 31, no. 6, pp. 6182–6193, 2017.
- [29] A. Avinash and A. Murugesan, "Prediction capabilities of mathematical models in producing a renewable fuel from waste cooking oil for sustainable energy and clean environment," *Fuel*, vol. 216, pp. 322–329, 2018.
- [30] S. Dharma, H. H. Masjuki, H. C. Ong et al., "Optimization of biodiesel production process for mixed *Jatropha curcas*-*Ceiba pentandra* biodiesel using response surface methodology," *Energy Conversion and Management*, vol. 115, pp. 178–190, 2016.
- [31] H. V. Lee, J. C. Juan, and Y. H. Taufiq-Yap, "Preparation and application of binary acid-base CaO-La<sub>2</sub>O<sub>3</sub> catalyst for biodiesel production," *Renewable Energy*, vol. 74, pp. 124–132, 2015.
- [32] H. Pan, L. Hu, X. F. Liu et al., "Mesoporous polymeric solid acid as efficient catalyst for (trans) esterification of crude *Jatropha curcas* oil," *Fuel Processing Technology*, vol. 150, pp. 50–57, 2016.
- [33] H. Li, S. Niu, C. Lu, and J. Li, "Calcium oxide functionalized with strontium as heterogeneous transesterification catalyst for biodiesel production," *Fuel*, vol. 176, pp. 63–71, 2016.
- [34] B. Changmai, I. B. Laskar, and L. Rokhum, "Microwave-assisted synthesis of glycerol carbonate by the transesterification of glycerol with dimethyl carbonate using *Musa acuminata* peel ash catalyst," *Journal of the Taiwan Institute of Chemical Engineers*, vol. 102, no. 2019, pp. 276–282, 2019.
- [35] C. Samart, P. Sreetongkittikul, and C. Sookman, "Heterogeneous catalysis of transesterification of soybean oil using KI/mesoporous silica," *Fuel Processing Technology*, vol. 90, no. 7–8, pp. 922–925, 2009.
- [36] S. B. Chavan, R. R. Kumbhar, D. Madhu, B. Singh, and Y. C. Sharma, "Synthesis of biodiesel from *Jatropha curcas* oil using waste eggshell and study of its fuel properties," *RSC Advances*, vol. 5, no. 78, pp. 63596–63604, 2015.
- [37] Y. T. Wang, Z. Fang, and F. Zhang, "Esterification of oleic acid to biodiesel catalyzed by a highly acidic carbonaceous catalyst," *Catalysis Today*, vol. 319, pp. 172–181, 2019.
- [38] A. F. Zanette, R. A. Barella, S. B. C. Pergher et al., "Screening, optimization and kinetics of *Jatropha curcas* oil transesterification with heterogeneous catalysts," *Renewable Energy*, vol. 36, no. 2, pp. 726–731, 2011.
- [39] K. F. Yee, K. T. Lee, R. Ceccato, and A. Z. Abdullah, "Production of biodiesel from *Jatropha curcas* L. oil catalyzed by SO<sub>2</sub>/ZrO<sub>2</sub> catalyst: effect of interaction between process variables," *Bioresource Technology*, vol. 102, no. 5, pp. 4285–4289, 2011.
- [40] K. F. Yee, J. C. S. Wu, and K. T. Lee, "A green catalyst for biodiesel production from *Jatropha* oil: optimization study," *Biomass and Bioenergy*, vol. 35, no. 5, pp. 1739–1746, 2011.
- [41] S. H. Teo, A. Islam, E. S. Chan et al., "Efficient biodiesel production from *Jatropha curcas* using CaSO<sub>4</sub>/Fe<sub>2</sub>O<sub>3</sub>-SiO<sub>2</sub> core-shell magnetic nanoparticles," *Journal of Cleaner Production*, vol. 208, pp. 816–826, 2019.
- [42] G. Kafuku, K. T. Lee, and M. Mbarawa, "The use of sulfated tin oxide as solid superacid catalyst for heterogeneous transesterification of *Jatropha curcas* oil," *Chemical Papers*, vol. 64, no. 6, pp. 734–740, 2010.
- [43] F. Zhang, Z. Fang, and Y. T. Wang, "Biodiesel production direct from high acid value oil with a novel magnetic carbonaceous acid," *Applied Energy*, vol. 155, pp. 637–647, 2015.
- [44] Y. T. Wang, Z. Fang, X. X. Yang et al., "One-step production of biodiesel from *Jatropha* oils with high acid value at low temperature by magnetic acid-base amphoteric nanoparticles," *Chemical Engineering Journal*, vol. 348, pp. 929–939, 2018.
- [45] F. Zhang, X. F. Tian, Z. Fang et al., "Catalytic production of *Jatropha* biodiesel and hydrogen with magnetic carbonaceous acid and base synthesized from *Jatropha* hulls," *Energy Conversion and Management*, vol. 142, pp. 107–116, 2017.
- [46] M. A. Olutoye and B. H. Hameed, "Synthesis of fatty acid methyl ester from crude *Jatropha (Jatropha curcas* Linnaeus) oil using aluminium oxide modified Mg-Zn heterogeneous catalyst," *Bioresource Technology*, vol. 102, no. 11, pp. 6392–6398, 2011.